THE JOURNAL OF PHYSICAL CHEMISTRY C

Article

pubs.acs.org/JPCC

Solving the Long-Standing Controversy of Long-Chain Alkanethiols Surface Structure on Au(111)

Xavier Torrelles,*[,†] Evangelina Pensa,[‡] Emiliano Cortés,[‡] Roberto Salvarezza,[§] Pilar Carro,[∥] Cecilia Hernández Guerrero,[†,⊥] Carmen Ocal,[†] Esther Barrena,[†] and Salvador Ferrer[#]

[†]Institute of Materials Science of Barcelona (ICMAB-CSIC), Campus UAB, Cerdanyola del Vallès 08193, Spain

[‡]Blackett Laboratory, Department of Physics, Imperial College London, SW7 2AZ London, United Kingdom

[§]The Research Institute of Theoretical and Applied Physical Chemistry (INIFTA), National University of La Plata-CONICET, La Plata 1900, Argentina

[∥]Department of Physical Chemistry, University of La Laguna, Institute of Materials and Nanotechnology, Avda. Francisco Sánchez, s/n 38071 La Laguna, Tenerife, Spain

[⊥]Department of Physics, University Autonomous of Barcelona (UAB), 08193 Bellaterra (Cerdanyola del Vallès), Barcelona, Spain

[#]ALBA Synchrotron Light Source, carrer de la Llum 2-26, 08290 Cerdanyola del Vallès, Barcelona, Spain

Supporting Information

ABSTRACT: The determination of the amount of gold adatoms and vacancies present at the thiol–gold interface of the $(\sqrt{3} \times \sqrt{3})$-R30° lattice on Au(111), usually observed for long-chain alkanethiols, is crucial to complete our knowledge on the species resulting from the thiol–substrate interaction. While this issue has been addressed for short and intermediate alkanethiols where Au adatom-complexes of the type RS–Au_{ad}–SR, known as staples, are formed, this issue is still under discussion for long-chain alkanethiols where different and contradictory models have been proposed. In this report we present X-ray diffraction data of the $(\sqrt{3} \times \sqrt{3})$-R30° structure for hexadecanethiol, allowing us to establish such basic structural features as the existence of Au adatoms and vacancies, the thiol adsorption-induced reconstruction of the surface, and the structure of the interface. These results allow us to reject the notion that vacancies and adatoms coexist within the same unit cell, and allow us to note that over the whole thiol–Au(111) interface the two exist in equal proportions. Vacancies appear on the gold surface as vacancy islands, and gold-adatoms appear flanked by two sulfur atoms, as observed on thiol-protected gold clusters and short thiols on Au(111). The coexistence of radicals and staples in the same $(\sqrt{3} \times \sqrt{3})$-R30° cell is consistent with experiment and theory.

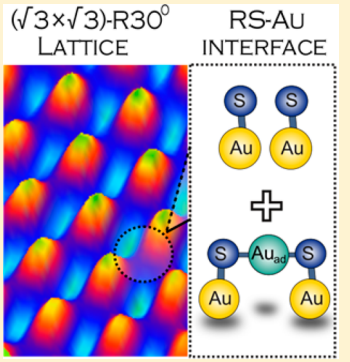

INTRODUCTION

Self-assembled monolayers (SAM) of alkanethiols and alkanedithiols on gold surfaces are still intensively studied given that revealing the exact chemical structure of this interface should shed light onto the self-assembling phenomena itself. This collaborative process finds numerous applications in various fields of materials science related to nanoscience, surface science, and inorganic chemistry including within bio- and nanotechnology for biological and medical applications,[1] chemical diagnostics,[2] molecular electronics,[3] passivation of gold nanoclusters,[4] surface patterning[5] and catalysis, among others.[6,7] Due to their relevance and the high number of applications, the thiol–gold system is considered an archetypal model system and consequently has been the focus of numerous structural studies with the aim of understanding the nature of the interaction between these molecules and the substrate's surface.[8−30]

It is widely accepted that the thiol–gold interaction results in the formation of strong gold–molecule bonds. However, how the thiol units bind to the surface is still under discussion.[31] The initial models in which thiol molecules would be simply bound as thiyl radicals to the Au surface at intermediate gold sites (i.e., fcc, hcp, and bridge)[32] was later questioned for numerous reasons: (1) the experimental proof that the thiol molecules are at a top site; (2) the incapability of this model to explain the presence of vacancy islands on the Au(111) surface after the thiol adsorption;[32] and (3) the determination of the interface structure for thiol-protected gold clusters,[33] which consists of gold atoms flanked by two sulfur atoms forming the so-called RS–Au–SR staple units (RS, SR: thiol units, where R = $(CH_2)_{n-1}CH_3$). For planar interfaces, the gold adatom in the staple unit might be an adatom extracted from the gold surface lattice unit, leaving a vacancy behind. The S-gold bond has a similar bonding strength to the gold–gold bond and therefore thiol adsorption can significantly modify the gold–gold bonding at the gold–sulfur interface. However, within this context, the chemical state of the Au adatom is still under debate.[34]

Received: November 29, 2017
Revised: January 24, 2018
Published: January 24, 2018

DOI: 10.1021/acs.jpcc.7b11465
J. Phys. Chem. C XXXX, XXX, XXX−XXX

Strong efforts have been recently made to explain the different surface structures in terms of staple units, in particular for the high coverage (3 × 4) and c(4 × 2) lattices, commonly observed for short and intermediate sized alkanethiols and the ($\sqrt{3}$ × $\sqrt{3}$)-R30° lattice typically observed for long alkanethiols.[32] While experimental data and theoretical calculations show that (3 × 4) and c(4 × 2) lattices can be satisfactorily described by RS−Au_{ad}−SR staple units exclusively,[35] the ($\sqrt{3}$ × $\sqrt{3}$)-R30° lattice may not be explained in terms of a model of simple staple units[32] since this lattice only contains a thiol molecule (RS) and 1/3 gold adatom per unit mesh while the staple needs two RS units. In fact, experimental data has been modeled considering different surface species upon this lattice structure: thyil radicals ($RS^{\bullet}$) adsorbed on different sites of the Au(111) surface,[36] RS−Au_{ad} moieties (0.33 adatom coverage, θ_{ad})[37] and 2 RS species and RS−Au_{ad}−SR moieties (0.08 adatom coverage) coexisting on the Au surface. The latter model involves homogeneously distributed vacancies produced by the Au_{ad} removal in a dynamical equilibrium and includes both vacancies and gold atoms in the unit cell.[21,38]

While these models explain some of features observed for the ($\sqrt{3}$ × $\sqrt{3}$)-R30° thiol lattice, they exhibit some important drawbacks. First, DFT calculations have shown that all these models for the ($\sqrt{3}$ × $\sqrt{3}$)-R30° lattice have a limited thermodynamic stability compared to that of the c(4 × 2) surface structure formed exclusively of RS−Au_{ad}−SR species.[32] This fact cannot explain the coexistence and dynamical equilibrium of these two lattices observed in many STM images giving clear evidence of very similar stabilities.[32] Second, they also fail to explain the 0.11−0.14 surface coverage of the gold vacancy islands (θ_{vac}), a figure close to 0.16 theoretically expected if the whole surface was covered with RS−Au_{ad}−SR species.[39] Thus, it is evident that a model for the ($\sqrt{3}$ × $\sqrt{3}$)-R30° surface structure should not only satisfy the condition of a similar stability as the c(4 × 2) lattice but also contain a large proportion of RS−Au_{ad}−SR species on the Au(111) surface to explain the vacancy island coverage observed by STM.

In order to solve this problem, it has been suggested that the interface of long alkanethiols retains the c(4 × 2) structure formed by staples with θ_{vac} = 0.16 while the ending thiol molecules appear as a ($\sqrt{3}$ × $\sqrt{3}$)-R30° phase[35] (i.e., the ($\sqrt{3}$ × $\sqrt{3}$)-R30° structure does not exist at the RS−Au interface). However, a theoretical model has been recently proposed for a ($3\sqrt{3}$ × $3\sqrt{3}$)-R30° structure[40] consisting of 3 RS-, thiyl radicals, and 3 RS−Au_{ad}−SR moieties formed by ($\sqrt{3}$ × $\sqrt{3}$)-R30° thiol lattice subunits that exhibits a thermodynamic stability similar to that shown by the c(4 × 2) lattice and θ_{vac} = 0.11, a value very close to experimental observations.[40] Note that the presence of adsorbed thiyls radicals has been proposed in many thiol−gold systems.[34] Therefore, it becomes essential to provide high-quality quantitative values of gold adatom and vacancy concentrations at the metal/molecule interface to support or reject not only this new ($3\sqrt{3}$ × $3\sqrt{3}$)-R30° model but also the previously published structural models. This is the central motivation of this letter.

While the presence of staples has been successfully established by STM for short alkanethiols on Au(111),[35] this technique fails to reveal the structure of the buried RS/Au interface of long alkanethiols. For these cases, diffraction can be used as the best suited technique. X-rays penetrate through an organic monolayer with negligible attenuation and consequently are sensitive to the inner structure of the monolayer as well as the monolayer/substrate interface; we may therefore unravel the nature of this interaction through the exact localization of the atoms at the interface. Our X-ray data reconciles with previous models, findings, and results in order to solve the longstanding problem of the S−Au interface for long-chain alkanethiols on Au(111).

The experiment was designed to give answers to fundamental questions concerning alkanethiol adsorption on Au(111) surface such as the following: Are RS−Au_{ad}−SR units present at the thiol−gold interface? What is the origin or source of the adatoms during the self-assembly process? Are there Au vacancies and Au adatoms on the ordered/disordered thiol areas? Answers to these questions would shed light on a key piece of this complex jigsaw and put us one step closer to complete our knowledge of the Au−S interface, the self-assembly process, and the link between planar and nanoparticle's local surface-chemistry and reactivity.

EXPERIMENTAL SECTION

The X-ray diffraction data was collected at the ID03 surface diffraction beamline of the European Synchrotron Radiation Facility, ESRF, Grenoble. Two experiments were performed on the same 1-hexadecanethiol (C16) on Au(111) system using similar experimental conditions and beam energies with the objective to accomplish a full data set.[41−43] The main difference between both data sets was the adjustment of the beam flux in order to reduce the radiation damage of the X-ray beam; as further supported in the text by comparing the surface coverage of the ($\sqrt{3}$ × $\sqrt{3}$)-R30° lattice in both cases. The X-ray beam was generated by three undulators (two U35 and one U32) and monochromatized with a liquid-nitrogen-cooled monolithic channel-cut Si(111) monochromator. Two mirrors, the first toroidal with controllable meridional radius and the second flat, initially focused the X-ray beam horizontally. A second Kirkpatrick−Baez mirror reduced the horizontal beam size to micrometer sizes at the sample position. The incident beam energy was set to 11.456 keV, lower than the Au L_{III} absorption edge to avoid the background due to the gold fluorescence. The Au(111) single crystal, with surface plane parallel to the crystallographic (111) planes within 0.1° of miscut as determined by X-ray diffraction measurements, was mounted in the UHV diffraction chamber (base pressure lower than 1 × 10^{-10} mbar) coupled with a six-circle diffractometer operated in the z-axis mode.[43] It was cleaned in an external UHV chamber by repeated cycles of ion sputtering and annealing up to 800 K until a well-developed (1 × 1) LEED diffraction pattern with sharp peaks was obtained. The sample was later immersed in 1 mM hexadecanethiol (C16, Sigma-Aldrich, 99%) ethanolic solution and annealed at 300 K for 24 h. Annealing at higher temperatures was avoided to prevent phase transitions.[44] This procedure permits the formation of a complete self-assembled monolayer (ML) of C16 with a surface coverage θ = 0.33. After a careful rinsing in ethanol to remove physisorbed molecules, the sample was transferred to the UHV diffraction chamber and cryogenically cooled at LN_2 temperature to reduce radiation damage. A fast shutter was also mounted to avoid unnecessary X-ray beam irradiation on the sample during noncounting periods. More detailed descriptions of the surface X-ray diffraction experiments, data acquisition, and refinement procedures are given in the Supporting Information.

In-air STM experiments were performed in the constant current mode with an ECM scanning probe microscope from Veeco Instruments (Bruker, Santa Barbara, CA) controlled by a

DOI: 10.1021/acs.jpcc.7b11465
J. Phys. Chem. C XXXX, XXX, XXX−XXX

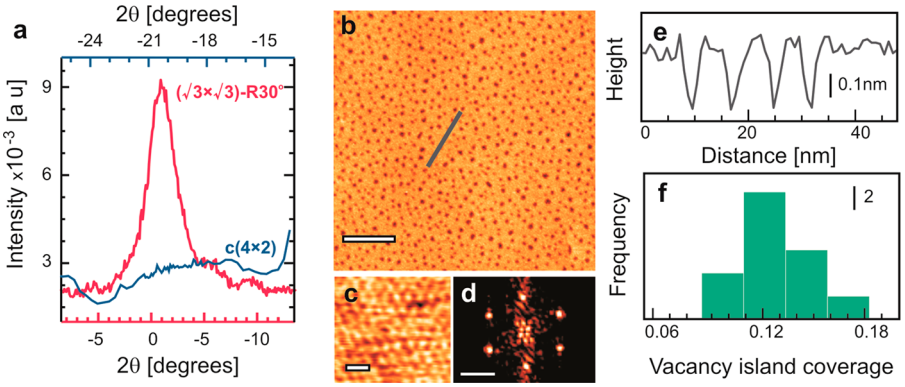

Figure 1. C16-SAM on Au(111). (a) High-resolution X-ray diffraction pattern corresponding to (red) the reflection (1/3, 1/3, 0.17), indicating the presence of the $(\sqrt{3} \times \sqrt{3})$-R30° lattice and (blue) the reflection (1/4, 0, 0.5) showing that no signal for c(4 × 2) lattice was detected. (b–f) In-air STM images and related data: (b) image showing the typical vacancies Au islands (dark features in the image) upon thiol adsorption. (c) High-resolution image evincing the $(\sqrt{3} \times \sqrt{3})$-R30° lattice. (d) FFT pattern corresponding to the STM image in c. (e) Height profile across gray line in image b making evident that Au vacancy islands only involve one atomic layer (i.e., 0.24 nm in height). (f) Histogram of the Au vacancy islands. The data was obtained from the analysis of many STM images of large, flat Au(111) terraces covered by the C16 SAM. Scale bars correspond to (b) 40 nm, (c) 1 nm, and (d) 2 nm^{-1}.

Nanoscope IIIA unit, also from Veeco Instruments. Mechanically cut Pt–Ir tips were used and typical bias voltages (E_{bias}), set-point currents, and scan rates were 0.5–0.8 V, 0.5–0.8 nA, and 1–30 Hz, respectively. The scanner calibration was checked by imaging highly oriented pyrolytic graphite (HOPG) with atomic resolution. WSxM software[45] was employed for imaging analysis. Samples were obtained by immersion of preferred oriented Au(111) substrates in the same conditions above-mentioned. The substrates were prepared by H_2 flame annealing of evaporated Au on chromium-coated glass plates (Arrandee, Germany).

RESULTS AND DISCUSSION

In order to reveal the atomistic arrangement of the S–Au interface for the $(\sqrt{3} \times \sqrt{3})$-R30° lattice, two X-ray diffraction experiments were performed under similar conditions on C16-SAMs on Au(111). These experiments complement each other to overcome the progressive suppression of the molecular ordering with X-ray exposure time due to radiation damage. We have selected C16, as both scanning probe images[46,47] and low-energy electron diffraction patterns[26,44] reveal that this alkanethiol is organized into $(\sqrt{3} \times \sqrt{3})$-R30° SAMs, as shown in Figure 1. In this way, for this alkanethiol chain-length, it is expected that the dominant contribution comes from the $(\sqrt{3} \times \sqrt{3})$-R30° lattice[26,44] rather than other possible surface structures (i.e., (3 × 4), c(4 × 2), etc.) usually found for shorter alkanethiol chain-lengths.[48]

One of the basic principles of diffraction technique, and crystallography as supported analysis technique, is its extreme sensitivity to periodic arrangements of elements present on the surface or in a crystal. Any regular ordering of elements forming a new periodicity on the surface (or bulk) will contribute with a typical set of reflections characteristic to this new periodicity (superstructure), and the intensities of the reflections will be related with the physical distribution of these elements in the new unit cell. On the basis of this assumption, if diffraction does not detect a superstructure, then this could be due to two reasons: Either the superstructure shows extremely small lateral domain sizes to be detected, or it is not present. In our experiments, the $(\sqrt{3} \times \sqrt{3})$-R30° is the only structure experimentally available (Figure 1a, red curve). No reflections intrinsic to other superstructures were detected, as exemplified in Figure 1a (blue curve) by the absences of the c(4 × 2) lattice's reflections. Moreover, STM molecular resolution images of C16-SAMs on the Au(111) also confirms the presence of the $(\sqrt{3} \times \sqrt{3})$-R30° structure (Figures 1c). Fast Fourier transform (FFT) analysis highlights the typical hexagonal pattern of the $(\sqrt{3} \times \sqrt{3})$-R30° structure (Figure 1d) and the absence of any other surface structure. For these reasons, we consider that the $(\sqrt{3} \times \sqrt{3})$-R30° average structure is the only one experimentally available and its structure is the one reported in the manuscript.

The $(\sqrt{3} \times \sqrt{3})$-R30° lattice was evidenced by the appearance of the corresponding specific reflections in the X-ray experiments. Its diffraction pattern is formed by an overlapping of patterns from the different $\sqrt{3}$-domains present at the surface (see Figure S1). Figure 1a shows the full width at half-maximum (fwhm) of reflections (1/3, 1/3, 0.17) and (2/3, 2/3, 0.17) were rather broad: 0.030 and 0.025 r.l.u. (reciprocal lattice units, see Supporting Information section 1 for further details), respectively, corresponding to ordered domain sizes of approximately 250 Å. This is in agreement with STM images of C16-SAMs on the Au(111) substrate. As it can be seen in Figure 1b, the appearance of vacancy islands (pits) reduces the long-range order of the SAM to tens of nm.[29,49,50]

Gaining further insight on the Au–S interface for the $(\sqrt{3} \times \sqrt{3})$-R30° lattice requires a deeper level of analysis of the X-ray diffraction data. In order to avoid technical details related to the technique itself, the modeling and the fitting, we have opted to summarize in this article the main procedures and results, leaving a big portion of the analysis in the Supporting Information.

The refinement of the surface structure by comparing between X-ray experiments and theoretical data from an atomic model involves fractional order reflections (FORs), that contain exclusively structural information on the $(\sqrt{3} \times \sqrt{3})$-R30° structure. Further information can be extracted from the analysis of the CTRs (Crystal Truncation Rods), which could have contributions of surfaces areas with both the $(\sqrt{3} \times \sqrt{3})$-R30° superstructure and unreconstructed areas (covered either by ordered or random distribution of molecules) following the same (1 × 1) lattice periodicity as the substrate cell).

The first structural objective was the search for a plausible host–guest model capable of refining both the integer and

DOI: 10.1021/acs.jpcc.7b11465
J. Phys. Chem. C XXXX, XXX, XXX–XXX

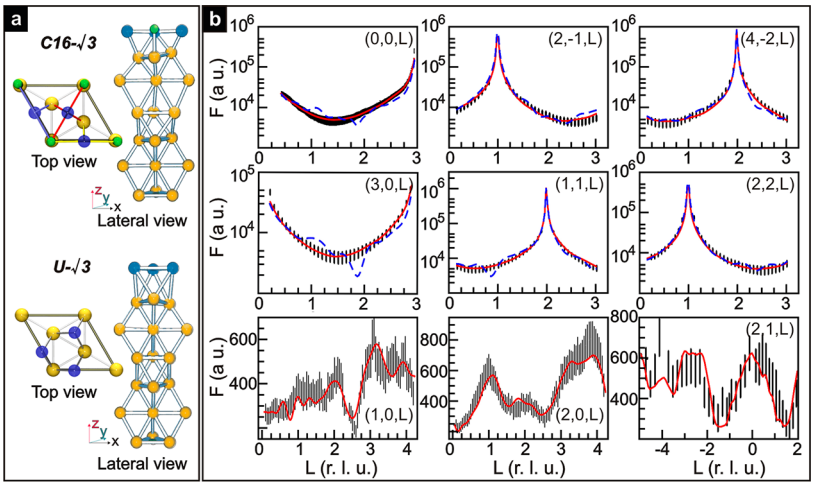

Figure 2. (a) Projected model along (x, z)-directions: [0$\bar{1}$1] and [111] directions of the fcc-gold crystal. Upper panel: Au(111)+S (**C16-$\sqrt{3}$** model with gold adatom in bridge position); lower panel: Au(111) (**U-$\sqrt{3}$** model with adatom in bulk position). The figure indicates the adatom layer (blue) and the S atom (green color), the thiol chain is not displayed. The gold interface is more distorted when the thiol molecules are ordered on the surface. The larger atomic distortions involve the topmost 5 gold surface layers (cf. Supporting Information sections 2−4 for more structural details). The gold adatom is placed in bulk or bridge positions for the **U-$\sqrt{3}$** or **C16-$\sqrt{3}$** cells, respectively. See text and Table S1 for more details. (b) Comparison between experimental and calculated data obtained from the best structural model that considers a surface covered with two different regions. The atomic coordinates of this model considering two different regions, i.e. **U-$\sqrt{3}$** + **C16-$\sqrt{3}$**, are given in Table S1 (red curves). The dashed blue curves are obtained from the best refinement process when the whole Au(111) surface is only covered with the ($\sqrt{3} \times \sqrt{3}$)-R30° superstructure, i.e., the **C16-$\sqrt{3}$** model/cell. See the text for the definition of **U-$\sqrt{3}$** model/cell.

fractional order rods, as shown in Figure S2. To achieve this goal, the CTRs and reflectivity curves were analyzed first (FORs were not considered at this initial stage) using an ideal bulk-terminated Au(111)-(1 × 1) surface. At this stage, the molecular thiol contribution to this data set was supposed negligible, as confirmed in the next paragraph. This initial modeling was performed in order to detect and quantify the percentage of gold vacancies and adatoms present at the Au(111) surface. This analysis shows the presence of a topmost gold layer with partial occupancy of θ_{ad} = 0.12 ± 0.01 plus a second deeper layer partially depleted by the same quantity, or equivalently, with atomic occupancy of 0.88 ± 0.01. This simple model with only one refined parameter (occupancy) was able to accomplish a χ^2 fit goodness factor close to 1, so it was taken as a reliable partial solution of the real surface structure. The refinement of the CTRs data set with this ideal (1 × 1) surface cell model and one parameter gives a calculated/experimental agreement almost identical to that shown in Figure 2b (red curves). The influence of this parameter is highlighted in Figure S3.

Since CTRs are sensitive to lateral order and a certain degree of order has been imposed to the fitted models, by considering a uniform average distribution of both vacancies and adatoms along the surface, the comparison between experimental and calculated data could show slight discrepancies. The real distribution of both adatoms and vacancies on the gold surface is not identical: Vacancies are grouped forming islands, and adatoms are uniformly distributed along the surface, both with identical surface coverage. This small difference could be the origin of these discrepancies observed in Figure S3. However, the reflectivity curve is not sensitive to lateral order, and its fitting clearly shows that the best solution can be achieved when the occupancy factors for adatoms and vacancies are both equal to 12% (Figure 2).

After finding a reliable solution for the topmost and second gold layers, the model was further expanded to a cell with ($\sqrt{3} \times \sqrt{3}$)-R30° periodicity. Two distinct ($\sqrt{3} \times \sqrt{3}$) cells were considered to account for areas of the surface covered with ordered and disordered or absent distribution of C16 molecules. The first model, defined as **C16-$\sqrt{3}$** cell from now on (Figure 2a, top), contains a C16 molecule on top of a gold atom and three gold adatoms, each of them with a partial occupancy value of 12% each. These adatoms are located in bridge position to simulate an average $\sqrt{3}$-structure of RS−Au_{ad}−SR staple units where the Au_{ad} is in bridge position and the S-units are on top. A top projection view of this model is shown in (Figure 2a, top). The blue balls correspond to each of the gold adatoms with an occupancy of 12% by $\sqrt{3}$-cell; consequently, only one gold adatom is present on the surface of every three $\sqrt{3}$-cells. Since the adatoms can randomly occupy each of the bridge positions as consequence of the surface symmetry, the positions of these three blue balls must be understood as possible directionalities of the staples, shown with different bond colors between S atoms (green) and gold adatoms (blue). The second model considers only three adatoms in bulk position with an occupancy of 12% each, to simulate the absence of staple units, the so-called **U-$\sqrt{3}$** cell/model (Figure 2a bottom). The top view of this model shows the three possible fcc-positions where the gold adatoms could be found in the $\sqrt{3}$-cell (blue) and which would match with those of an equivalent layer located 3 levels deeper. Both models contribute to the CTRs subset of data set, however, only the **C16-$\sqrt{3}$** one contributes to the FORs subset. In this way, $F_{CTRs} = \theta F_{C16\text{-}\sqrt{3}} + (1 - \theta) F_{U\text{-}\sqrt{3}}$ where the bulk contribution is already accounted in each of the terms and θ indicates the corresponding surface coverage of each phase.

Refinement of the **C16-$\sqrt{3}$** cell/model considering the total coverage (θ = 1 or 100%) of the gold surface was not able to reduce the χ^2 fit goodness factor of the CTRs subset of data to values lower than 1.5 (dashed blue line in Figure 2b). The best refinement of the CTRs data set was obtained using the two cells (**C16-$\sqrt{3}$+U-$\sqrt{3}$**) to account the progressive lost of the

DOI: 10.1021/acs.jpcc.7b11465
J. Phys. Chem. C XXXX, XXX, XXX−XXX

$\sqrt{3}$-molecular ordering due to radiation damage (see Supporting Information for details on radiation damage) and the continuous increasing of the unreconstructed (or molecularly disordered) surface coverage with CTRs measuring time. After this measuring process, the surface could only be fitted with the unreconstructed model, accounting for 96% of the total coverage ($\theta-1 = 0.96$). This value indicates that the **U-$\sqrt{3}$** cell would cover the majority of the gold-surface and would not be reconstructed or equivalently would show the (1 × 1) periodicity of the bulk gold surface and could take into account a disordered distribution of molecules on the surface with no effective contribution to the diffraction data (except at background level through diffuse scattering). The term molecular disorder is in this case assigned to a structure showing such small lateral domain sizes that they do not contribute to the diffraction pattern or to the presence of molecules on the surface without lateral translation periodicity (molecules with undefined neighbor distances, presence of molecules with different orientations and/or molecules with collapsed chains on the surface, and molecules placed on different substrate sites, among others). Despite this molecular disordering, the average (1 × 1) distribution of gold vacancies and adatoms present at the surface remains unchanged, as mentioned previously (CTRs fitted with an ideal bulk-terminated Au(111)-(1 × 1) surface model). For this reason, a second experiment was carried out under different experimental conditions to increase the lifetime of the ($\sqrt{3}$ × $\sqrt{3}$)-R30° molecular ordering on the surface. These experimental conditions enabled us to measure a larger and complementary data set to the previous one, as will be discussed later on in this section.

The final model, defined as **U-$\sqrt{3}$+C16-$\sqrt{3}$**, is compatible with the presence of alkanethiol chains on the whole gold surface (ordered or disordered) that are responsible for the vacancies on the topmost surface layer whose atoms move up forming a partial gold ad-layer on top with identical occupancy coverage among themselves, such that the vacancy coverage is similar to the adatoms coverage. The use of identical cell sizes permits us to identify where the adatoms are located (or at least on average) on both surfaces, unreconstructed and reconstructed. The position of the Au_{ad} is expected to be the same (or close) in both cells. The details on the parameters used for each model as well as those related to the structural refinement procedure and errors associated with the measurements and fitting are given in the Supporting Information sections 2–4.

The magnitude of disordered C16 regions contrasts with IR data, which reveals a crystalline-like sample with the CH_2 asymmetric stretching at 2915 cm^{-1}.[51] This disorder is caused by the X-ray beam radiation damage as confirmed after acquiring a second data set measured under softer radiation conditions and adjusted using both the **U-$\sqrt{3}$** and **C16-$\sqrt{3}$** cells. The intensity profiles of the CTRs from both data sets are different, which is to be expected due to their different **U-$\sqrt{3}$** and **C16-$\sqrt{3}$** covering fraction ratios. The **U-$\sqrt{3}$+C16-$\sqrt{3}$** model was used to refine a data set similar to that of Figure 2b but measured using conditions that caused lower levels of radiation damage to the sample (Figure S4). The scale factors as well as the atomic coordinates of the Au atoms of both models were also slightly readjusted. In this case, the surface-covering factor of ordered **C16-$\sqrt{3}$** thiol regions was $\theta = 0.66$. The information derived from both data sets (or experiments) supports the presence of Au adatoms at the surface and vacancies on the topmost surface level (i.e., localized at layers Au_{1i} and Au_{2i} in Table S1, respectively).

The **U-$\sqrt{3}$+C16-$\sqrt{3}$** model was used to refine the total SXRD-data by means of least-squares minimum procedures (LSQ). The χ^2 fit goodness factor of our best-fit solution is 0.5 and corresponds to the model drawn in Figure 3, where several views are given: (left) lateral and (right) top, corresponding to the final surface structure. See the Supporting Information for more details on the refinement procedure. Figure 3 shows the adatom in bridge position because the goodness fit factor remains similar when supposing the adatom in bulk or bridge positions as will be commented below.

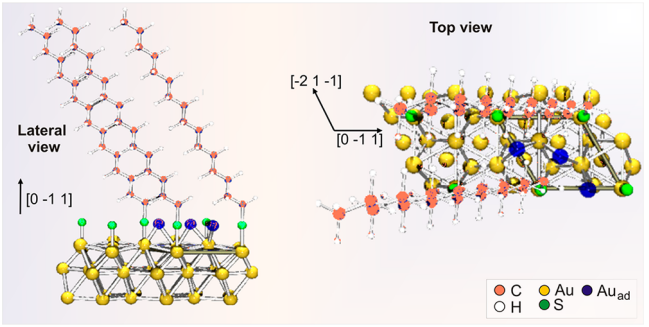

Figure 3. Lateral (left) and top (right) views of the final structure. A surface slab containing two ($\sqrt{3}$ × $\sqrt{3}$)-R30° cells is depicted with indication of the hexagonal cell at the right side of each figure. The three blue atoms contained in the ($\sqrt{3}$ × $\sqrt{3}$)-R30° cell correspond with the three possible equivalent positions where the gold adatom could site in the unit cell. The atomic occupancy of each blue atom is 12% similar to that previously obtained for the adatom of the Au(111)-(1 × 1) surface. Their positions out of the cell have been omitted for clarity. Only 1/3 of gold adatom is present by ($\sqrt{3}$ × $\sqrt{3}$)-R30°-cell. Green atoms correspond to sulfur atoms in thiol chains. In top panel, only two C16-thiol chains are drawn for clarity at (x, y) = (0,0) bottom left and (1,1) upper right corners of the unit cell, respectively. In bottom figure (lateral view) only 3 of the 6 thiol chains present in the two ($\sqrt{3}$ × $\sqrt{3}$)-R30°-cells of the slab are drawn to avoid overlap projections between different chains: (x, y): (0, 0), (1, 0), and (0, 1).

In light of the structural results of the C16/Au(111) interface highlighted within the previous section, the following points are confirmed.

Origin of Gold Adatoms and Vacancy Islands on the Gold (111) Surface Is Related to the Presence of Thiol Molecules. The analysis of the experimental CTRs highlights only the average structure of the Au(111) surface since they only contain the average (1 × 1) structure of both the **U-$\sqrt{3}$** and the **C16-$\sqrt{3}$** cells. Consequently, the information derived can be easily extrapolated to the whole surface. In this case, the analysis indicates the presence of an added layer on top of the outermost gold surface layer with a coverage θ_{ad}= 0.12 ± 0.01 and a deficiency of atoms on the outermost gold of ($1 - \theta_{ad}$) (i.e., θ_{vac} = 0.12 ± 0 0.01). This value is independent from the surface-covering factor of the **C16-$\sqrt{3}$** superstructure. In fact, the same θ_{ad} value was obtained after refining the structures with data sets shown in Figures 2b and S4, where the thiol coverage values were 4 and 66%, respectively. These results indicate that the formation of vacancies and adatoms on the gold surface is due to the presence of molecules with independency of their ordering, in agreement with our STM

DOI: 10.1021/acs.jpcc.7b11465
J. Phys. Chem. C XXXX, XXX, XXX−XXX

molecular resolution images of the ($\sqrt{3} \times \sqrt{3}$)-R30° structure for C16-SAMs on the Au(111) as shown in Figures 1c.

Presence of Vacancy Islands and Gold Adatoms on Covered Thiol Areas. The analysis of both CTRs and FORs points out the presence of gold adatoms in both ordered and disordered regions of the Au(111) substrate. The **C16-$\sqrt{3}$** model is compatible with the presence of $\theta_{ad} = 0.12 \pm 0.01$ on the topmost surface, and 1/3 Au_{ad} without vacancies in the unit cell. This model seems in disagreement with those of references[21,37,38] since they assume that the gold vacancies are included in their respective unit cells[21,38] and consequently are not able to explain the presence of vacancy islands over the entire Au(111) surface, as revealed in the STM images (Figures 1b/f and S5). Moreover, the proposed model in ref 38 is not able to explain the experimental data with the basic ($\sqrt{3} \times \sqrt{3}$)-R30° unit cell since it lacks of translation periodicity due to disorder. An expansion of the ($\sqrt{3} \times \sqrt{3}$)-R30° cell to a ($3\sqrt{3} \times 3\sqrt{3}$)-R30° supercell is needed to explain their XRD data. In this case, the concentration of adatoms is similar to ours (1/3 Au_{ad} per ($\sqrt{3} \times \sqrt{3}$)-R30° cell), but the number of vacancies needed is double (0.66 gold vacancies per ($\sqrt{3} \times \sqrt{3}$)-R30° cell). In contrast, ref 37 does not show gold vacancies in the surface and contains as many adatoms as molecules.

In fact, experimental data (CTRs and reflectivity) is not compatible with monatomic vacancies models of the gold surface as these models should account for the presence of $\theta_{vac} \approx 0.10$ determined from STM images[39,52] plus a random distribution of individual gold vacancies inside each ($\sqrt{3} \times \sqrt{3}$)-R30° cell. This situation would imply a higher number of atomic vacancies at the surface than $\theta_{vac} = 0.12$ derived from our model. In the case of a surface fully covered with the ($\sqrt{3} \times \sqrt{3}$)-R30°-phase, the surface coverage factor would be $\theta_{vac} \approx 0.24$ (i.e. 0.12 from the vacancy islands associated with STM images plus 0.12 from individual gold vacancies localized in each ($\sqrt{3} \times \sqrt{3}$)-R30° mesh). Consequently, the 0.12 of vacancies derived from our data analysis can only be associated with the similar proportion of vacancy islands that are observed by STM (Figures 1f and S5). This means that as thiol adsorption takes places and individual vacancies are formed by Au atom removal the individual vacancies diffuse to form the Au vacancy islands.

Other models proposed in the literature supposing an interface retaining a c(4 × 2) structure while ending thiol molecules appear as a ($\sqrt{3} \times \sqrt{3}$)-R30°-phase[35] can be disregarded due to the total absence of detectable reflections intrinsic to the c(4 × 2) structure in our experimental data (as shown in Figure 1a). Also, in the model proposed in ref 35 the SAM is composed by "all staples" so that $\theta_{ad} = 0.16$ is expected, in contrast with $\theta_{ad} = 0.12$ experimentally observed in our work. It can be argued that 0.04 Au_{ad} should be provided by the lifting of the herringbone reconstruction. This ejection of adatoms do not generate vacancies associated with them. However, capturing these additional 0.04 Au_{ad} by the RS species would lead to 0.16 RS−Au_{ad}−SR species and accordingly to the c(4 × 2) superstructure, a fact that it is not observed in the experimental data (Figure 1a). Moreover, it is evident that these 0.04 Au_{ad} (with no vacancies associated) are not included in the 0.12 vacancy/0.12 Au_{ad} balance find it in our experimental results. Why are these Au_{ad} not incorporated into the thiol lattices? One explanation is that the ($\sqrt{3} \times \sqrt{3}$)-R30° structure containing a mixture of RS−Au_{ad}−SR and RS species becomes more stable as the hydrocarbon chain is increased.[40] Therefore, the affinity of the system for incorporating more Au_{ad} decreases. One can speculate that this excess of Au_{ad} should be incorporated at the step edges.

C16 Site Adsorption: Top versus hcp/fcc. Since the second data set displayed in Figure S4 shows a higher molecular coverage (66%) than the first in Figure 2b (4%), it has been used to check whether the CTRs are sensitive or not to the site position of the C16 molecules. The results of this test are shown in the Supporting Information section 4.2. The data refinement (CTRs + FORs) clearly shows a good fit when the C16 molecule is positioned on top (of similar quality as that shown in Figure 2a for the first data set) with a goodness fit factor $\chi^2_{top} = 1.1$. The refinement procedure, however, becomes unstable when forcing the molecule to remain on hcp/fcc positions. In these cases, the refinement of the CTRs generates larger gold relaxations (blue curve in Figure S4), which modify rather poorly the agreement between experimental and calculated FORs. The goodness fit factor in the hcp case takes a value three times larger than top case, $\chi^2_{hcp} = 3.1$. This fact, consequently, rules out the hcp C16-adsorption site. Similar discussion can be applied for the fcc adsorption site; in this case, however, the goodness fit factor is even worse than in the previous two cases: $\chi^2_{fcc} = 5.0$. Therefore, we conclude that the molecule is adsorbed at top site, in agreement with previous data,[33,53−55] with a S−Au bond length of 2.28 ± 0.02 Å. Note that the top site adsorption and the S−Au bond length are consistent with the presence of staples (RS−Au_{ad}−SR) and adsorbed RS radicals.[40]

In summary, the results derived from the presented experiments offer complementary information on the role of the C16 molecules on the Au(111) surface. When the ordered C16 coverage is low, the C16/gold interface shows a vacancy/adatom distribution that extends to the disordered C16 regions, suggesting that this relation is independent of the molecular ordering, at least after exposure to X-rays. The vacancy/adatom distribution is independent of the ordered C16 coverage fraction, as demonstrated after analysis of the second data set, suggesting the absence of vacancies (but not of adatoms) on the C16/($\sqrt{3} \times \sqrt{3}$)-R30° regions. In fact, these results turn STM and X-rays measurements compatible between them.

Finally, the bonding of the sulfur headgroup is localized on the top site upon the gold substrate. The refinement of the data placing the molecule in top/hcp/fcc only shows a reasonable agreement factor between experimental and calculated data for the top position.

($\sqrt{3} \times \sqrt{3}$)-R30° Surface Structure. Our results on the ($\sqrt{3} \times \sqrt{3}$)-R30° structure show a surface cell containing 1 molecule in top position and 1/3 gold adatom. The presence of a fraction of atom in the unit cell reflects the disordered nature of its structure (1 gold adatom is shared between three ($\sqrt{3} \times \sqrt{3}$)-R30°-cells), so it could be extrapolated to a larger and periodic cell as the ($3\sqrt{3} \times 3\sqrt{3}$)-R30° structure that maintains the same stoichiometry of vacancies and gold adatoms on the surface than the ($\sqrt{3} \times \sqrt{3}$)-R30° for theory calculation purposes. This 9-fold larger cell displayed in Figure 4a (not experimentally observed) has been recently shown to be energetically stable and contains 3 gold adatoms (blue atoms in Figure 4a) covering the surface by 11%, similar to that detected in our experiment.[40]

The average structure of the ($3\sqrt{3} \times 3\sqrt{3}$)-R30° theoretical model shows minor structural differences from the ($\sqrt{3} \times \sqrt{3}$)-R30° model as the position of the Au_{ad} varies within the cell: either bridge (Figure 4a) or fcc sites (bulk), respectively.

DOI: 10.1021/acs.jpcc.7b11465
J. Phys. Chem. C XXXX, XXX, XXX−XXX

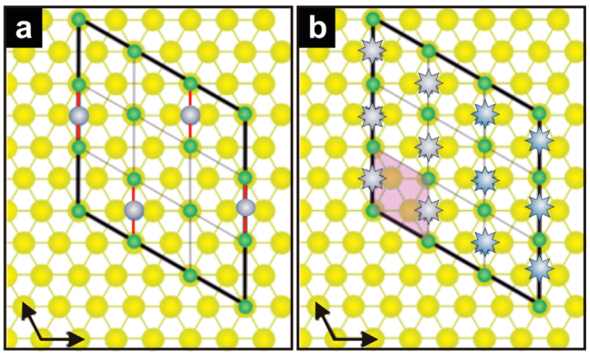

Figure 4. (a) Thiols/Au(111)-($3\sqrt{3} \times 3\sqrt{3}$)-R30° superstructure model. Thiol chains are omitted for clarity. Color identifiers: gold substrate (yellow), sulfur atom (green), and gold adatoms (blue). The vertical red lines interconnecting sulfur and gold adatoms identify RS–Au_{ad}–SR staple units. (b) Average structure of the previous model. Each gold adatom position has been averaged between the equivalent sites of each of the nine ($\sqrt{3} \times \sqrt{3}$)-R30° cells (shared unit) forming the ($3\sqrt{3} \times 3\sqrt{3}$)-R30° mesh. Each of the 9 gold adatoms (blue symbols) has an occupancy factor of 1/3.

This different location of the gold adatoms in their respective atomic cells gives different goodness fit factors between them. However, this difference reduces to a value close to 7% when the average ($3\sqrt{3} \times 3\sqrt{3}$)-R30° model (Figure 4b) is refined and the 12 domains considered. This small discrepancy still makes the model refinement acceptable due to the experimental uncertainties (see Supporting Information section 4).

The X-ray diffraction measurements presented in this work were performed on freshly prepared samples and only the presence of a ($\sqrt{3} \times \sqrt{3}$)-R30° phase with equal vacancies coverage and gold adatoms on the Au(111) surface and close to 0.12 was detected. In the previous section ("C16 Site Adsorption: Top versus hcp/fcc"), we conclude that gold vacancies concentrate forming islands on the surface and not individual gold site vacancies on the ($\sqrt{3} \times \sqrt{3}$)-R30° cell. From these results and those obtained from STM experiments on surfaces where the ($\sqrt{3} \times \sqrt{3}$)-R30° and c(4 × 2) phases coexist and calculations are already present in the literature, a global overview of the role of the ($\sqrt{3} \times \sqrt{3}$)-R30° structure on the Au(111) surface could be envisaged:

(1) According to the presence of vacancies and adatoms on the Au(111) surface, the ($\sqrt{3} \times \sqrt{3}$)-R30° cell must be able to take adatoms from the Au surface and annihilates the single atom vacancies forming, as detected in our case, vacancy islands.

(2) Since the chemisorption of RS species on the gold surface is responsible of taking adatoms from it, the RS–Au_{ad}–SR staple units must already be intrinsically contained in the ($\sqrt{3} \times \sqrt{3}$)-R30° average surface structure (i.e., 1/3 adatom per ($\sqrt{3} \times \sqrt{3}$)-R30° cell). This θ_{ad} value means that there is one Au_{ad} interacting with two thiol molecules every three $\sqrt{3}$-cells, or in other words, the $\sqrt{3}$-structure contains a staple unit every three cells (one ($\sqrt{3} \times \sqrt{3}$)-R30° cell contains the adatom while other two not); consequently, in the ($\sqrt{3} \times \sqrt{3}$)-R30° cell coexist two different types of molecules: staple units and thyil radicals.

(3) The strong constrain imposed by the chains orientation forming the staple could induce short- and long-range order in molecular orientation but not necessarily spatial periodicity of the staples along the surface.

(4) The basic unit formed by three ($\sqrt{3} \times \sqrt{3}$)-R30° cells would not show long-range order even if statistically two or more neighboring cells contain one staple each, as a consequence of the fixed adatoms coverage on the surface (1/3 adatom per ($\sqrt{3} \times \sqrt{3}$)-R30° cell).

(5) An ordered distribution of three $\sqrt{3}$-cells with ratio 1:2 (one cell with adatom and the other two empty) has not been experimentally observed: (a) During the initial formation of the staple in the unit cell, the adatom can be placed between three equivalent positions in the ($\sqrt{3} \times \sqrt{3}$)-R30° cell (nearest neighboring thiol molecules: Figure 3, top view). (b) The adatoms coverage on the surface statistically fixes the average concentration ratio 1:2 of filled and empty cells, consequently the spatial ordering of neighboring ($\sqrt{3} \times \sqrt{3}$)-R30° cells giving place to long-range order would not be guaranteed (i.e. (F, E, E) = (E, F, E) = (E, E, F) where each bracket refers to three ($\sqrt{3} \times \sqrt{3}$)-R30° cells, F = filled and E = empty cell (with or without adatom, respectively)). The spatial distribution along the surface of each of these units would have equal probability.

(6) Height profiles on STM molecular resolution images (see Supporting Information section 6) show that the ($\sqrt{3} \times \sqrt{3}$)-R30° phase displays two well-defined heights, which can be consequence of two different types of thiol molecules coexisting in the structure: staple units and thyil radicals.[47,56] In ref 40, DFT calculations on a ($3\sqrt{3} \times 3\sqrt{3}$)-R30° ordered surface model containing 3 staples and 3 thyil molecules as that shown in Figure 4a, using thiols with different chain lengths (hexanethiol, octadecanethiol, and undecanethiol), shows that the height difference between both molecule specimens for the three chain lengths varies from 0.08 to 0.1 Å.[40] This is in agreement with the average value obtained from the height profile analysis of high-resolution STM images in Figures S6 and S7. The higher height corresponds to the molecules of the staple units while the lower one to the thyil radicals, both sited on top position (cf. Supporting Information section 6).

(7) The ($\sqrt{3} \times \sqrt{3}$)-R30° structure does not appear to be thermodynamically stable since it is an average structure of another (the probe is that each ($\sqrt{3} \times \sqrt{3}$)-R30° cell shares one Au_{ad} with other two) and has no periodic order beyond the ($\sqrt{3} \times \sqrt{3}$)-R30° cell. As mentioned previously, DFT energy stability calculations performed on an ordered ($3\sqrt{3} \times 3\sqrt{3}$)-R30° superstructure,[40] suggests that (a) for long thiol chains (n > 13) the stability differences between the c(4 × 2) and the ($3\sqrt{3} \times 3\sqrt{3}$)-R30° cells are very small and (b) the interchain van der Waals interaction would be better optimized for this last cell together with a lesser cost of energy per alkanethiol to form a Au_{ad}. This study summarizes that these results would slightly favor the ($3\sqrt{3} \times 3\sqrt{3}$)-R30° surface lattice over the c(4 × 2). In the case of the ($\sqrt{3} \times \sqrt{3}$)-R30° structure, van der Waals forces between neighbor chains could also be a driving force for stabilizing the interaction between chains with similar orientation (induced by the staples). These constraints could certainly have the effect of reducing the surface mobility toward the formation of the c(4 × 2) at room temperature.[39,57]

(8) Even if the cost/gain energy already calculated for the ($3\sqrt{3} \times 3\sqrt{3}$)-R30° structure is similar to that of the c(4 × 2), it could be considered as an intermediate structure between the disordered ($\sqrt{3} \times \sqrt{3}$)-R30° cell and the stable c(4 × 2) attending to the amount of adatoms per unit cell (i.e., 1/3 for the ($3\sqrt{3} \times 3\sqrt{3}$)-R30° and 1/2 for the c(4 × 2) structures, respectively) and to the tendency for the c(4 × 2) to be formed from the ($\sqrt{3} \times \sqrt{3}$)-R30° cell.[32]

DOI: 10.1021/acs.jpcc.7b11465
J. Phys. Chem. C XXXX, XXX, XXX–XXX

CONCLUSIONS

Overall, our results clarify the structure of the $(\sqrt{3} \times \sqrt{3})$-R30° thiol-Au(111) interface frequently observed with long thiols. The most relevant information concerns the amount of adatom/vacancies coexisting within the $(\sqrt{3} \times \sqrt{3})$-R30° thiol lattice. The data analysis of the two experiments concluded that once the $\sqrt{3}$-cell covers the surface the distribution of gold vacancies and adatoms is 12% for both of them and that this distribution remains on the surface even after the molecular ordering disappears.

This information has a direct impact upon the previous models proposed for this elusive system. In fact, the adatom coverage θ_{ad} = 0.12 experimentally estimated in this article is clearly inconsistent with the RS−Au model that implies θ_{ad} = 0.33.[37] Moreover, our results allow us to discard the dynamical model[38] that predicts θ_{ad} = 0.08, and the two site model that does not include adatom/vacancies.[53] Also, the absence of reflections corresponding to the c(4 × 2) buried interface allows to discard the model proposed in ref 35 for the $(\sqrt{3} \times \sqrt{3})$-R30° lattice of long alkanethiols. The quantification of an amount of gold adatoms in the $(\sqrt{3} \times \sqrt{3})$-R30° cell by X-rays implies the coexistence of two different thiol specimens in the unit cell, staple and thyil radicals, placed on top sites that are in line with STM height profiles analysis and DFT calculations. The X-ray results are compatible with the average structure of the $(3\sqrt{3} \times 3\sqrt{3})$-R30° model as consequence of the minor structural differences with respect to the $(\sqrt{3} \times \sqrt{3})$-R30° model, mainly localized on the site position of the gold adatoms in their respective unit cell mesh.

ASSOCIATED CONTENT

Supporting Information

The Supporting Information is available free of charge on the ACS Publications website at DOI: 10.1021/acs.jpcc.7b11465.

Detailed sections on experimental methods, model construction, set of parameters used for describing the structural models, structural refining procedures and detailed surface and interface structure description, radiation damage on the sample and experimental STM images and line profile analysis confirming the experimental findings (PDF)

AUTHOR INFORMATION

Corresponding Author

*E-mail: torrelles@icmab.es.

ORCID

Xavier Torrelles: 0000-0002-6891-7793

Emiliano Cortés: 0000-0001-8248-4165

Roberto Salvarezza: 0000-0002-7617-4539

Carmen Ocal: 0000-0001-8790-8844

Esther Barrena: 0000-0001-9163-2959

Notes

The authors declare no competing financial interest.

ACKNOWLEDGMENTS

X.T. acknowledges financial support from the Spanish Ministry of Economy and Competitiveness through the "Severo Ochoa" Programme for Centres of Excellence in R&D (SEV-2015-0496). R.C.A. acknowledges financial support from ANPCyT (PICT 2010-2554) from Argentina. P.C. acknowledges MINECO (ENE2016-74889-C4-2-R, AEI-FEDER-UE). We also acknowledge the European Synchrotron Radiation Facility for provision of synchrotron radiation facilities and we would like to thank Drs. M. Jankowski and H. Isern for assistance using beamline. X.T., E.P., and E.C. acknowledge financial support from ESRF.

REFERENCES

(1) Demers, L. M.; Ginger, D. S.; Park, S.-J.; Li, Z.; Chung, S.-W.; Mirkin, C. A. Direct Patterning of Modified Oligonucleotides on Metals and Insulators by Dip-Pen Nanolithography. *Science* **2002**, *296*, 1836−1838.

(2) Otsubo, T.; Aso, Y.; Takimiya, K. Functional Oligothiophenes as Advanced Molecular Electronic Materials. *J. Mater. Chem.* **2002**, *12*, 2565−2575.

(3) Heimel, G.; Romaner, L.; Zojer, E.; Bredas, J.-L. The Interface Energetics of Self-Assembled Monolayers on Metals. *Acc. Chem. Res.* **2008**, *41*, 721−729.

(4) Badia, A.; Singh, S.; Demers, L.; Cuccia, L.; Brown, G. R.; Lennox, R. B. Self-Assembled Monolayers on Gold Nanoparticles. *Chem. - Eur. J.* **1996**, *2*, 359−363.

(5) Xia, Y. N.; Whitesides, G. M. Soft lithography. *Annu. Rev. Mater. Sci.* **1998**, *28*, 153−184.

(6) Whetten, R. L.; Shafigullin, M. N.; Khoury, J. T.; Schaaff, T. G.; Vezmar, I.; Alvarez, M. M.; Wilkinson, A. Crystal Structures of Molecular Gold Nanocrystal Arrays. *Acc. Chem. Res.* **1999**, *32*, 397−406.

(7) Ulman, A. Formation and Structure of Self-Assembled Monolayers. *Chem. Rev.* **1996**, *96*, 1533−1554.

(8) Heaven, M. W.; Dass, A.; White, P. S.; Holt, K. M.; Murray, R. W. Crystal Structure of the Gold Nanoparticle $[N(C_8H_{17})_4]$-$[Au_{25}(SCH_2CH_2Ph)_{18}]$. *J. Am. Chem. Soc.* **2008**, *130*, 3754−3755.

(9) Jadzinsky, P. D.; Calero, G.; Ackerson, C. J.; Bushnell, D. A.; Kornberg, R. D. Structure of a Thiol Monolayer-Protected Gold Nanoparticle at 1.1 Å Resolution. *Science* **2007**, *318*, 430−433.

(10) Qian, H.; Eckenhoff, W. T.; Zhu, Y.; Pintauer, T.; Jin, R. Total Structure Determination of Thiolate-Protected Au38 Nanoparticles. *J. Am. Chem. Soc.* **2010**, *132*, 8280−8281.

(11) Zeng, C.; Qian, H.; Li, T.; Li, G.; Rosi, N. L.; Yoon, B.; Barnett, R. N.; Whetten, R. L.; Landman, U.; Jin, R. Total Structure and Electronic Properties of the Gold Nanocrystal $Au_{36}(SR)_{24}$. *Angew. Chem.* **2012**, *124*, 13291−13295.

(12) Crasto, D.; Malola, S.; Brosofsky, G.; Dass, A.; Häkkinen, H. Single Crystal XRD Structure and Theoretical Analysis of the Chiral $Au_{30}S(S\text{-}t\text{-}Bu)_{18}$ Cluster. *J. Am. Chem. Soc.* **2014**, *136*, 5000−5005.

(13) Das, A.; Li, T.; Nobusada, K.; Zeng, C.; Rosi, N. L.; Jin, R. Nonsuperatomic $[Au_{23}(SC_6H_{11})_{16}]-$ Nanocluster Featuring Bipyramidal Au15 Kernel and Trimeric $Au_3(SR)_4$ Motif. *J. Am. Chem. Soc.* **2013**, *135*, 18264−18267.

(14) Zeng, C.; Li, T.; Das, A.; Rosi, N. L.; Jin, R. Chiral Structure of Thiolate-Protected 28-Gold-Atom Nanocluster Determined by X-ray Crystallography. *J. Am. Chem. Soc.* **2013**, *135*, 10011−10013.

(15) Nimmala, P. R.; Knoppe, S.; Jupally, V. R.; Delcamp, J. H.; Aikens, C. M.; Dass, A. $Au_{36}(SPh)_{24}$ Nanomolecules: X-ray Crystal Structure, Optical Spectroscopy, Electrochemistry, and Theoretical Analysis. *J. Phys. Chem. B* **2014**, *118*, 14157−14167.

(16) Zeng, C.; Chen, Y.; Liu, C.; Nobusada, K.; Rosi, N. L.; Jin, R. Gold tetrahedra coil up: Kekulé-like and double helical superstructures. *Science Adv.* **2015**, *1*, e1500425.

(17) Dass, A.; Theivendran, S.; Nimmala, P. R.; Kumara, C.; Jupally, V. R.; Fortunelli, A.; Sementa, L.; Barcaro, G.; Zuo, X.; Noll, B. C. Au133(SPh-tBu)52 Nanomolecules: X-ray Crystallography, Optical, Electrochemical, and Theoretical Analysis. *J. Am. Chem. Soc.* **2015**, *137*, 4610−4613.

(18) Azubel, M.; Koivisto, J.; Malola, S.; Bushnell, D.; Hura, G. L.; Koh, A. L.; Tsunoyama, H.; Tsukuda, T.; Pettersson, M.; Häkkinen, H.; Kornberg, R. D. Electron Microscopy of Gold Nanoparticles at Atomic Resolution. *Science* **2014**, *345*, 909−912.

DOI: 10.1021/acs.jpcc.7b11465
J. Phys. Chem. C XXXX, XXX, XXX−XXX

(19) Voznyy, O.; Dubowski, J. J.; Yates, J. T.; Maksymovych, P. The Role of Gold Adatoms and Stereochemistry in Self-Assembly of Methylthiolate on Au(111). *J. Am. Chem. Soc.* **2009**, *131*, 12989−12993.
(20) Grönbeck, H.; Häkkinen, H.; Whetten, R. L. Gold−Thiolate Complexes Form a Unique c(4 × 2) Structure on Au(111). *J. Phys. Chem. C* **2008**, *112*, 15940−15942.
(21) Cossaro, A.; Mazzarello, R.; Rousseau, R.; Casalis, L.; Verdini, A.; Kohlmeyer, A.; Floreano, L.; Scandolo, S.; Morgante, A.; Klein, M. L.; Scoles, G. X-ray Diffraction and Computation Yield the Structure of Alkanethiols on Gold(111). *Science* **2008**, *321*, 943−946.
(22) Love, J. C.; Estroff, L. A.; Kriebel, J. K.; Nuzzo, R. G.; Whitesides, G. M. Self-Assembled Monolayers of Thiolates on Metals as a Form of Nanotechnology. *Chem. Rev.* **2005**, *105*, 1103−1170.
(23) Laibinis, P. E.; Whitesides, G. M.; Allara, D. L.; Tao, Y. T.; Parikh, A. N.; Nuzzo, R. G. Comparison of the Structures and Wetting Properties of Self-Assembled Monolayers of n-Alkanethiols on the Coinage Metal Surfaces, Copper, Silver, and Gold. *J. Am. Chem. Soc.* **1991**, *113*, 7152−7167.
(24) Vericat, C.; Vela, M. E.; Corthey, G.; Pensa, E.; Cortes, E.; Fonticelli, M. H.; Ibanez, F.; Benitez, G. E.; Carro, P.; Salvarezza, R. C. Self-Assembled Monolayers of Thiolates on Metals: a Review Article on Sulfur-Metal Chemistry and Surface Structures. *RSC Adv.* **2014**, *4*, 27730−27754.
(25) Strong, L.; Whitesides, G. M. Structures of Self-Assembled Monolayer Films of Organosulfur Compounds Adsorbed on Gold Single Crystals: Electron Diffraction Studies. *Langmuir* **1988**, *4*, 546−558.
(26) Dubois, L. H.; Zegarski, B. R.; Nuzzo, R. G. Molecular Ordering of Organosulfur Compounds on Au(111) and Au(100): Adsorption from Solution and in Ultrahigh Vacuum. *J. Chem. Phys.* **1993**, *98*, 678−688.
(27) Chidsey, C. E. D.; Liu, G. Y.; Rowntree, P.; Scoles, G. Molecular Order at the Surface of an Organic Monolayer Studied by Low Energy Helium Diffraction. *J. Chem. Phys.* **1989**, *91*, 4421−4423.
(28) Alves, C. A.; Smith, E. L.; Porter, M. D. Atomic Scale Imaging of Alkanethiolate Monolayers at Gold Surfaces with Atomic Force Microscopy. *J. Am. Chem. Soc.* **1992**, *114*, 1222−1227.
(29) Fenter, P.; Schreiber, F.; Berman, L.; Scoles, G.; Eisenberger, P.; Bedzyk, M. J. On the Structure and Evolution of the Buried S/Au Interface in Self-Assembled Monolayers: X-ray Standing Wave Results. *Surf. Sci.* **1998**, *412*−*413*, 213−235.
(30) Grumelli, D.; Cristina, L. J.; Maza, F. L.; Carro, P.; Ferrón, J.; Kern, K.; Salvarezza, R. C. Thiol Adsorption on the Au(100)-hex and Au(100)-(1 × 1) Surfaces. *J. Phys. Chem. C* **2015**, *119*, 14248−14254.
(31) Reimers, J. R.; Ford, M. J.; Marcuccio, S. M.; Ulstrup, J.; Hush, N. S. Competition of van der Waals and Chemical Forces on Gold−Sulfur Surfaces and Nanoparticles. *Nature Rev. Chem.* **2017**, *1*, 0017.
(32) Vericat, C.; Vela, M. E.; Benitez, G.; Carro, P.; Salvarezza, R. C. Self-Assembled Monolayers of Thiols and Dithiols on Gold: New Challenges for a Well-Known System. *Chem. Soc. Rev.* **2010**, *39*, 1805−1834.
(33) Hakkinen, H. The Gold-Sulfur Interface at the Nanoscale. *Nat. Chem.* **2012**, *4*, 443−455.
(34) Reimers, J. R.; Ford, M. J.; Halder, A.; Ulstrup, J.; Hush, N. S. Gold Surfaces and Nanoparticles are Protected by Au(0)−Thiyl Species and Are Destroyed When Au(I)−Thiolates Form. *Proc. Natl. Acad. Sci. U. S. A.* **2016**, *113*, E1424−E1433.
(35) Guo, Q.; Li, F. Self-Assembled Alkanethiol Monolayers on Gold Surfaces: Resolving the Complex Structure at the Interface by STM. *Phys. Chem. Chem. Phys.* **2014**, *16*, 19074−19090.
(36) Vericat, C.; Lenicov, F. R.; Tanco, S.; Andreasen, G.; Vela, M. E.; Salvarezza, R. C. Building Complex Two−Dimensional Structures: Methylene Blue on Self-Assembled Monolayer−Covered Au(111). *J. Phys. Chem. B* **2002**, *106*, 9114−9121.
(37) Yu, M.; Bovet, N.; Satterley, C. J.; Bengió, S.; Lovelock, K. R. J.; Milligan, P. K.; Jones, R. G.; Woodruff, D. P.; Dhanak, V. True Nature of an Archetypal Self-Assembly System: Mobile Au-Thiolate Species on Au(111). *Phys. Rev. Lett.* **2006**, *97*, 166102.
(38) Mazzarello, R.; Cossaro, A.; Verdini, A.; Rousseau, R.; Casalis, L.; Danisman, M. F.; Floreano, L.; Scandolo, S.; Morgante, A.; Scoles, G. Structure of a CH_3S Monolayer on Au(111) Solved by the Interplay between Molecular Dynamics Calculations and Diffraction Measurements. *Phys. Rev. Lett.* **2007**, *98*, 016102.
(39) Pensa, E.; Cortés, E.; Corthey, G.; Carro, P.; Vericat, C.; Fonticelli, M. H.; Benítez, G.; Rubert, A. A.; Salvarezza, R. C. The Chemistry of the Sulfur−Gold Interface: In Search of a Unified Model. *Acc. Chem. Res.* **2012**, *45*, 1183−1192.
(40) Carro, P.; Torrelles, X.; Salvarezza, R. C. A Novel Model for the $(\sqrt{3}\times\sqrt{3})$-R30° Alkanethiolate-Au(111) Phase Based on Alkanethiolate-Au Adatom Complexes. *Phys. Chem. Chem. Phys.* **2014**, *16*, 19017−19023.
(41) Ferrer, S.; Comin, F. Surface Diffraction Beamline at ESRF. *Rev. Sci. Instrum.* **1995**, *66* (2), 1674−1676.
(42) Comin, F. A Cryogenically Cooled, Sagittal Focusing Scanning Monochromator for ESRF. *Rev. Sci. Instrum.* **1995**, *66*, 2082−2084.
(43) Balmes, O.; van Rijn, R.; Wermeille, D.; Resta, A.; Petit, L.; Isern, H.; Dufrane, T.; Felici, R. The ID03 Surface Diffraction Beamline for In-Situ and Real-Time X-ray Investigations of Catalytic Reactions at Surfaces. *Catal. Today* **2009**, *145*, 220−226.
(44) Fenter, P.; Eisenberger, P.; Liang, K. S. Chain-Length Dependence of the Structures and Phases of $CH_3(CH_2)_n$ SH Self-Assembled on Au(111). *Phys. Rev. Lett.* **1993**, *70*, 2447−2450.
(45) Horcas, I.; Fernández, R.; Gómez-Rodríguez, J. M.; Colchero, J.; Gómez-Herrero, J.; Baro, A. M. WSXM: A Software for Scanning Probe Microscopy and a Tool for Nanotechnology. *Rev. Sci. Instrum.* **2007**, *78*, 013705.
(46) Morita, S.; Wiesendanger, R.; Meyer, E. *Noncontact Atomic Force Microscopy*; Springer: Berlin Heidelberg, 2012.
(47) Fukuma, T.; Kobayashi, K.; Horiuchi, T.; Yamada, H.; Matsushige, K. Alkanethiol Self-Assembled Monolayers on Au(111) Surfaces Investigated by Non-Contact AFM. *Appl. Phys. A: Mater. Sci. Process.* **2001**, *72*, S109−S112.
(48) Carro, P.; Pensa, E.; Vericat, C.; Salvarezza, R. C. Hydrocarbon Chain Length Induces Surface Structure Transitions in Alkanethiolate−Gold Adatom Self-Assembled Monolayers on Au(111). *J. Phys. Chem. C* **2013**, *117*, 2160−2165.
(49) Mamun, A. H. A.; Hahn, J. R. Effects of Solvent on the Formation of Octanethiol Self-Assembled Monolayers on Au(111) at High Temperatures in a Closed Vessel: A Scanning Tunneling Microscopy and X-ray Photoelectron Spectroscopy Study. *J. Phys. Chem. C* **2012**, *116*, 22441−22448.
(50) Cavalleri, O.; Hirstein, A.; Bucher, J.-P.; Kern, K. Ordering Processes at the Decanethiol Au(111) Interface. *Thin Solid Films* **1996**, *284*−*285*, 392−395.
(51) Grumelli, D.; Méndez De Leo, L. P.; Bonazzola, C.; Zamlynny, V.; Calvo, E. J.; Salvarezza, R. C. Methylene Blue Incorporation into Alkanethiol SAMs on Au(111): Effect of Hydrocarbon Chain Ordering. *Langmuir* **2010**, *26*, 8226−8232.
(52) Kautz, N. A.; Kandel, S. A. Alkanethiol Monolayers Contain Gold Adatoms, and Adatom Coverage Is Independent of Chain Length. *J. Phys. Chem. C* **2009**, *113*, 19286−19291.
(53) Torrelles, X.; Vericat, C.; Vela, M. E.; Fonticelli, M. H.; Daza Millone, M. A.; Felici, R.; Lee, T.-L.; Zegenhagen, J.; Muñoz, G.; Martín-Gago, J. A.; Salvarezza, R. C. Two-Site Adsorption Model for the $(\sqrt{3}\times\sqrt{3})$-R30° Dodecanethiolate Lattice on Au(111) Surfaces. *J. Phys. Chem. B* **2006**, *110*, 5586−5594.
(54) Kondoh, H.; Iwasaki, M.; Shimada, T.; Amemiya, K.; Yokoyama, T.; Ohta, T.; Shimomura, M.; Kono, S. Adsorption of Thiolates to Singly Coordinated Sites on Au(111) Evidenced by Photoelectron Diffraction. *Phys. Rev. Lett.* **2003**, *90*, 066102.
(55) Woodruff, D. P. The Interface Structure of n-Alkylthiolate Self-Assembled Monolayers on Coinage Metal Surfaces. *Phys. Chem. Chem. Phys.* **2008**, *10*, 7211−7221.
(56) Poirier, G. E.; Tarlov, M. J. The c(4 × 2) Superlattice of n-Alkanethiol Monolayers Self-Assembled on Au(111). *Langmuir* **1994**, *10*, 2853−2856.

DOI: 10.1021/acs.jpcc.7b11465
J. Phys. Chem. C XXXX, XXX, XXX−XXX

933 (57) Barrena, E.; Ocal, C.; Salmeron, M. Evolution of the Structure
934 and Mechanical Stability of Self-Assembled. *J. Chem. Phys.* **1999**, *111*,
935 9797.

DOI: 10.1021/acs.jpcc.7b11465
J. Phys. Chem. C XXXX, XXX, XXX−XXX